coatings

MDPI

Article

Design and Corrosion Resistance Performance of Nano-Multilayer Coatings for the Protection of Breathing Gas Cylinders Used in Diving

Feng Yuan [1], Yunjiang Yu [2], Yuekai Li [1], Yanxiong Xiang [2] and Changwei Zou [2,*]

[1] School of Physical Education, Lingnan Normal University, Zhanjiang 524048, China; yuanf@lingnan.edu.cn (F.Y.)
[2] School of Physics Science and Technology, Lingnan Normal University, Zhanjiang 524048, China; yanxiongxiang@163.com (Y.X.)
* Correspondence: zoucw@lingnan.edu.cn

Abstract: Seamless gas cylinders for diving exhibit excellent low-temperature impact performance, lightweight characteristics, and good corrosion resistance, making them widely applicable in underwater activities. However, during use, the peeling of paint or corrosion on the surface of these cylinders poses a significant threat to their safety. In this study, environmentally friendly arc ion plating technology was used to deposit TiBN, CrAlN, and nano-multilayer coatings of CrAlN/TiBN. The surface morphology, tribological properties, and corrosion resistance of these coatings were investigated. The results indicated that both CrAlN and CrAlN/TiBN coatings possess fewer droplets, pinholes, and pits, and the cross-section of the CrAlN/TiBN coating exhibits a denser structure. The preferred orientation for TiBN was identified as TiB_2 (101), while that for CrAlN was Cr(Al)N (200), with the preferred orientation for CrAlN/TiBN being TiB_2 (101). The friction measurements revealed that the lowest coefficient was observed in the CrAlN/TiBN coating (0.489), followed by CrAlN (0.491) and then TiBN (0.642). Electrochemical tests conducted in artificial seawater demonstrated that the self-corrosion potential was highest for the CrAlN/TiBN coating, followed by CrAlN and lastly TiBN. The developed TiBN-based nano-multilayer coatings hold substantial application value in protecting seamless gas cylinders used in diving.

Keywords: seamless gas cylinders for diving; arc ion plating; CrAlN/TiBN; corrosion resistance performance

Citation: Yuan, F.; Yu, Y.; Li, Y.; Xiang, Y.; Zou, C. Design and Corrosion Resistance Performance of Nano-Multilayer Coatings for the Protection of Breathing Gas Cylinders Used in Diving. *Coatings* **2024**, *14*, 1435. https://doi.org/10.3390/coatings14111435

Academic Editors: Jordan Todorov Maximov and Galya Velikova Duncheva

Received: 8 October 2024
Revised: 4 November 2024
Accepted: 5 November 2024
Published: 12 November 2024

1. Introduction

The seamless diving cylinders are known for their excellent low-temperature impact performance, lightweight design, and good corrosion resistance, making them widely applicable in diving activities [1,2]. Corrosion can weaken the strength and durability of these cylinders, making them more susceptible to physical damage such as cracking or deformation. This not only increases safety risks during use but may also lead to the premature retirement of the cylinder, resulting in higher replacement frequency and costs. Moreover, if the anti-corrosive layer on either the interior or exterior of the cylinder is compromised, gas may leak from damaged areas. This not only wastes valuable resources but could also pose potential hazards to both environmental health and human safety [3]. Peeling paint or corrosion on the outer surface can significantly reduce the compressive strength, bending resistance of the wall, and overall corrosion resistance—factors that greatly affect the integrity of the cylinder. Such conditions can easily lead to internal explosions within the cylinder, posing serious risks to personal safety [4]. Additionally, due to prolonged exposure in seawater environments, these alloy seamless cylinders are particularly prone to corrosive reactions which can substantially shorten the lifespan of critical components such as valves and regulators. The primary causes of corrosion in seamless breathing cylinders

include seawater corrosion, crevice corrosion, and electrochemical corrosion. Materials exposed to marine environments may experience accelerated wear due to a synergistic effect between various forms of deterioration rather than solely from individual factors like simple corrosion or frictional wear [5–8].

The chromate passivation process exhibits excellent corrosion resistance and stable performance, having been applied in the industry for many years. However, due to the carcinogenicity, diffusivity, and bioaccumulation of Cr(VI), it poses significant threats to both environmental safety and human health. Therefore, developing high-corrosion-resistant chromium-free passivation processes is of great importance. The protective coatings prepared by the physical vapor deposition (PVD) technology exhibit excellent density and adhesion, which can coat the substrate surface with micro-level metal or non-metal compounds that are insoluble and exhibit outstanding corrosion resistance and wear resistance [9,10]. The composition and outcomes of these protective coatings have evolved from initial single-layer coatings to multi-layered, gradient-coated, nano-multilayer structures. Among these advancements, nano-multilayers have gained attention due to their superior wear resistance, strong adhesion between film and substrate, good corrosion resistance, high hardness, and long service life [11]. In recent years, nano-composite TiBN coatings have demonstrated high hardness, excellent toughness, low friction, and good chemical stability, making them potential candidates for wear-resistant protective coatings [12]. However, many of these reports lack depth in their investigation of the lubrication mechanisms associated with TiBN/base lubricating systems [12]. They do not comprehensively consider the system design perspective, particularly regarding the mechanical properties of the films that significantly influence the solid–liquid composite system and their effects on friction and wear performance [13]. In addition to these properties, TiBN coatings also exhibit significant advantages in marine corrosion resistance. The nano-hardness of TiBN coatings (ranging from 24 GPa to 34.5 GPa) strongly depends on the dual-phase structure of TiN/(amorphous) BN [12]. At lower N_2 partial pressures, deposited TiBN coatings can achieve hardness values up to 40 GPa due to the formation of a metastable solid solution where B dissolves in face-centered cubic (FCC) TiN. Further increasing the N_2 partial pressure leads to the formation of a nano-composite material with a hardness of approximately 30 GPa composed of both TiN and BN [13]. The addition of element B effectively reduces the grain size, significantly enhances the hardness of TiN coatings, and maintains good toughness, thereby avoiding the brittleness associated with BN and TiB_2 coatings.

Research indicates that ternary CrAlN coatings are particularly noteworthy because they possess high hardness, toughness, extended lifespan, strong abrasive wear resistance capabilities, as well as robust corrosion resistance and chemical stability [14]. Additionally, studies suggest that Cr_2O_3 formed from chromium can serve a lubricating role by reducing friction [15]. Adesina A.Y. et al. [16] employed cathodic arc ion plating technology to deposit TiN, CrN, CrAlN, and TiAlN coatings on 304 stainless steel and investigated the corrosion behavior of these coatings in a corrosive medium consisting of 3.5% NaCl solution. The results indicated a significant positive shift in self-corrosion potential for all four coated samples compared to the 304 stainless steel substrate. Electrochemical impedance spectroscopy revealed that compared to similar nitrides formed via magnetron sputtering techniques, the deposited layers exhibited enhanced abilities against defect propagation and pore expansion when immersed in 3.5% NaCl solution. The addition of B elements in CrN-based coatings has become another focal point of research. However, single-layer coatings tend to grow continuously during the deposition process, which can lead to a columnar structure, allowing corrosive media to easily penetrate the coating material and even corrode the substrate, significantly reducing the corrosion resistance of the coating. To address this challenge, designing multilayer structures presents an effective method for enhancing both corrosion resistance and wear performance. Since the preparation process of multilayer coatings involves alternating deposition, differences in thermal expansion coefficients or lattice constants between different layers can result in

dislocation stacking at the interfaces, which can hinder the formation of columnar structures within any given layer [17]. Yu et al. [18] utilized arc ion plating technology to fabricate CrYN/TiBN coatings and indicated that with increasing additions of Ti and B elements, both columnar growth and dense structures were eliminated, leading to a face-centered cubic CrN structure and amorphous BN structure being formed. The grain size was reduced from 33 nm to 15 nm, resulting in a denser coating that exhibited improved friction and wear performance.

Currently, there are relatively few research reports on CrAlN/TiBN nanocomposite multilayer coatings, and the investigation of their corrosion behavior in seawater environments remains to be explored. Therefore, this study employs arc ion plating technology to prepare TiBN, CrAlN, and CrAlN/TiBN multilayer coatings. A systematic examination is conducted on the evolution of the microstructural morphology of the coatings, their tribological properties, as well as their electrochemical corrosion behavior in artificial seawater and potential applications for protective measures in underwater gas cylinders.

2. Experimental Details

2.1. Coating Preparation Process

In our preliminary work, CrN, CrTiN, CrWN/MoN nano-multilayer, and CrTiBN coatings were deposited onto 316 stainless steel substrates using multi-arc ion plating techniques [19,20]. The coating equipment used in this study is the AS510DTXB arc ion plating system produced by Danpu Company (Beijing, China). The single-side polished 304 stainless steel and single-crystal silicon were used as the substrates. Taking CrAlN/TiBN nano-multilayer coatings as an example, prior to coating, the substrate was cleaned using a metal cleaning agent followed by deionized water and anhydrous ethanol, undergoing ultrasonic cleaning for 20 min before being dried. The substrate was then mounted onto a sample holder using fixtures. The entire sample base can perform unidirectional rotation, while the holder on top allows for two-dimensional self-rotation. The target materials utilized for depositing film layers include the TiB_2 target (99.9 at.% with a Ti to B atomic ratio of 33:67), Cr target (99.99 at.%), and CrAl composite target (99.9 at.% with a Cr to Al atomic ratio of 30:70). Before deposition, the chamber was heated to 400 °C and evacuated to achieve base vacuum conditions while maintaining a rotational speed of 1 r/min for the substrate. Argon gas was introduced, adjusting pressure to 2 Pa, and a negative bias voltage of −1000 V on the substrate was applied as the ion source activates with power set at 6 kW for glow discharge cleaning treatment lasting 30 min. Subsequently, the bias voltage was adjusted to −800 V in vacuum priority mode, with a working pressure set at 0.7 Pa and the current maintained at a fixed value of 80 A. Following this step, we adjusted the bias voltage to −100 V while introducing nitrogen gas under vacuum priority mode with the working pressure set at 3.0 Pa. After closing off from further deposition from the Cr target while maintaining the pressure at 3.0 Pa, both CrAl and TiB_2 targets are activated simultaneously with their respective currents set accordingly. Specific deposition parameters are detailed in Table 1.

Table 1. Deposition parameters for coating.

Coatings	Base Pressure / 10^{-3}Pa	Experimental Pressure /Pa	Temperature /°C	Substrate Bias /V	TiB_2 Arc Current /A	CrAl Arc Current /A	Rotation /r·min^{-1}	Coating Time/min
TiBN	5.0	0.7	400	100	70	70	1	60
CrAlN	5.0	0.7	400	100	70	70	1	60
TiBN/CrAlN	5.0	0.7	400	100	70	70	1	60

2.2. Characterization of Coating Properties

The JSM-7610F field emission scanning electron microscope (SEM, JEOL, Tokyo, Japan) was employed to analyze the surface and cross-sectional micro-morphology of the coatings.

The microstructural study was conducted using the X'Pert Pro X-ray diffractometer from Nalytical, Almelo, The Netherlands, with a Cu-K radiation source. The step size was set at 0.02°, and the sample scanning range (2θ) spans from 10° to 80°. For friction performance testing, we employed the MFT-4000 multifunctional material surface performance tester manufactured by Lanzhou Huahui Instrument Technology Co., Ltd., Lanzhou, China. In a dry environment, experiments were carried out using a 4 mm stainless steel ball under a load of 10 N and a sliding speed of 200 mm/min over a reciprocating distance of 5 mm for a duration of 60 min. The test conditions maintain an ambient temperature and relative humidity of 24 °C and 61%, respectively.

To simulate corrosive environments akin to marine conditions for workpieces, we utilized the Corrtest-CS350 electrochemical workstation produced by Wuhan Kest Company, Wuhan, China. The electrochemical corrosion performance tests were performed using a standard three-electrode system where artificial seawater serves as the corrosive medium. The main components are listed in Table 2. The auxiliary electrode consists of platinum foil, while the working electrode comprises the tested samples. Additionally, a saturated KCl solution silver/silver chloride reference electrode was used. Three types of coatings underwent sequential open circuit potential (OCP) testing, electrochemical impedance spectroscopy (EIS), and polarization curve analysis (Tafel). The OCP measurement lasted for 3600 s, while the EIS scan frequencies ranged from 0.01 Hz to 100 kHz with a constant amplitude sine signal set at ±5 mV. Finally, polarization curves were obtained through dynamic potential scans within −1 V to +1.5 V at a scan rate of 0.001 V/s.

Table 2. Main components of artificial seawater.

(g/L) NaCl	$MgCl_2$	Na_2SO_4	$CaCl_2$	KCl	$NaHCO_3$
24.53	5.20	4.09	1.16	0.695	0.201

3. Results and Discussion

3.1. Microstructure of Coatings

Figure 1 shows the XRD spectra for the 304 stainless steel substrate, TiBN coating, CrAlN coating, and CrAlN/TiBN multilayer coating. It is noteworthy that all these coatings exhibit a cubic close-packed structure. The preferred orientations of the CrAlN and TiBN coatings were (200) and (111), respectively. On the other hand, it appears that the TiBN coating primarily consists of TiB_2 with its (111) crystal phase. Interestingly, we find that the XRD patterns for both the CrAlN/TiBN multilayer coating and TiBN coating are quite similar which can be attributed to variations in elemental composition, specifically concerning Ti, B, Cr, and N during deposition. However, it was important to note that coatings tend to grow along their lowest energy crystal planes, and a preferred orientation for the CrAlN/TiBN multilayer aligned with the TiB_2 (101) plane was observed [21–23]. It is also worth mentioning that diffraction peaks corresponding to body-centered cubic phases such as those from (200) and (111) planes of Cr(Al)N are notably absent from our observations of the CrAlN/TiBN multilayer. This absence may be due to either excessively fine grain sizes or insufficient crystallinity within other crystalline phases present in these coatings, leading to challenges in detecting corresponding characteristic peaks within our XRD pattern.

The surface and facture cross-sectional SEM morphologies of TiBN, CrAlN, and CrAlN/TiBN coatings are presented in Figure 2. As illustrated in Figure 2(a1–c1), all three types of coatings display common growth defects typically found in arc ion-plated films, including pinholes, droplets, and craters. Such phenomena occur during the coating preparation process due to variations in arc spot movement and uneven heating of the target material. These factors can lead to localized melting on the target surface, resulting in molten pools that release larger liquid particles, and these particles then collide with and adhere to the substrate surface, forming irregular aggregates [16,24]. The presence of large particles, pinholes, and craters on the coating surface tends to increase roughness

while potentially reducing the film and substrate adhesion strength, which may ultimately result in delamination. Moreover, it is noteworthy from Figure 2(a1–c1) that the TiBN coating exhibits a higher density of large particles along with noticeable pits when compared to both CrAlN and CrAlN/TiBN coatings, which show fewer large particles and pits. This distinction can be attributed to the formation of amorphous or nanocrystalline borides at the surfaces of TiBN as well as CrAlN/TiBN coatings, which enhances their overall density [25]. The analysis of Figure 2b reveals that the CrAlN coating exhibits a relatively loose, typical columnar crystal structure. In contrast, the TiBN coating shown in Figure 2(a2) demonstrates a denser structure compared to that of the CrAlN coating depicted in Figure 2(b2). When incorporating TiBN compounds into the CrAlN coating, the resulting CrAlN/TiBN layer is more compact than its single-component counterpart CrAlN. This phenomenon may be attributed to the incorporation of boron (B) elements, which exist as solid solutions within both the Cr(Al)N and TiN phases, leading to lattice distortion that partially hinders columnar crystal growth. Furthermore, regarding coating thickness, under identical deposition times, it was observed that the deposition rate for these coatings is as follows: $v_{TiBN/CrAlN} > v_{CrAlN} > v_{TiBN}$.

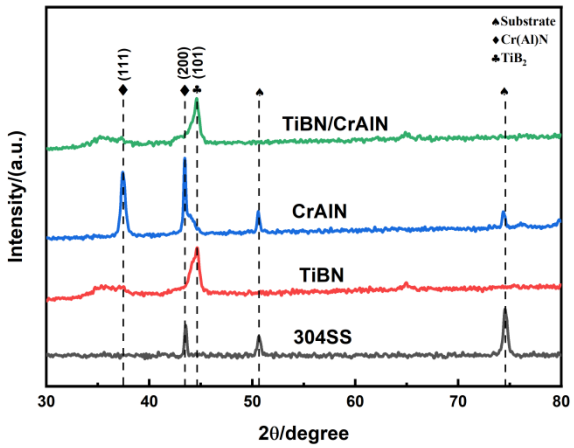

Figure 1. XRD patterns of 304 stainless steel, TiBN, CrAlN, and CrAlN/TiBN coatings.

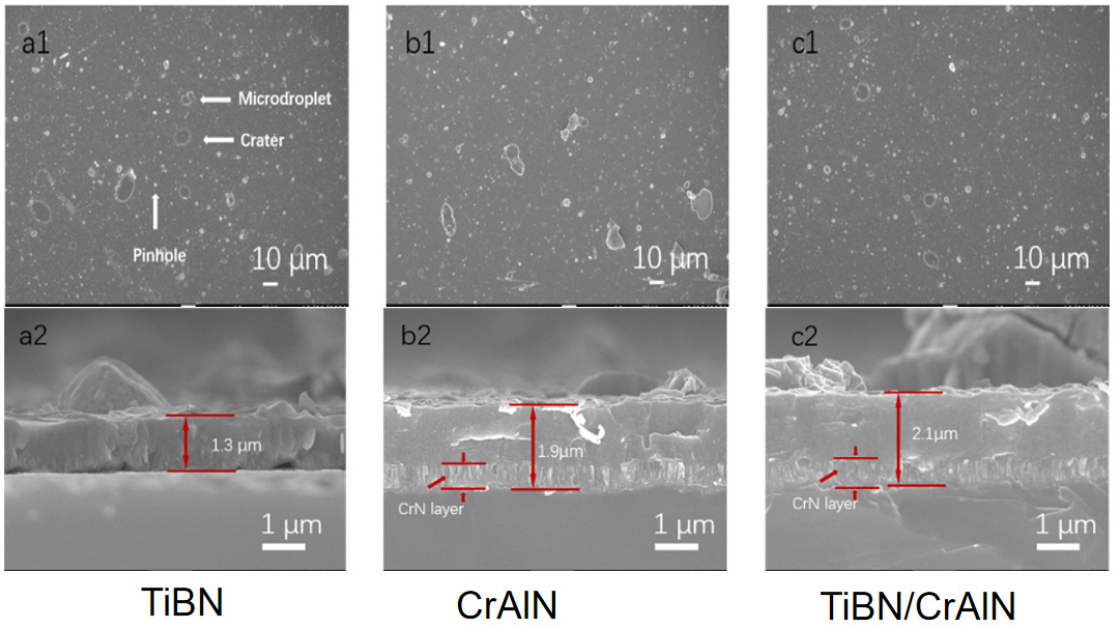

Figure 2. Surface and cross-sectional SEM images of TiBN (**a1**,**a2**), CrAlN (**b1**,**b2**), and CrAlN/TiBN (**c1**,**c2**) coatings.

3.2. Tribological Properties of Coatings

Figure 3 presents the friction curves for the various coatings we examined. It is evident from this figure that during the initial minute of the friction test (running-in period), all four samples exhibit rapid fluctuations in their coefficients of friction before settling around a more stable value. This behavior may be attributed to the presence of irregular large particles and pits on the coating surface, which contribute to an increase in roughness [26–29]. As wear progresses over time, organic contaminants and hard abrasive particles are either worn away or become embedded within the coatings, resulting in a gradual decrease in the coefficient of friction. Notably, for CrAlN coatings, there is a slight reduction in this coefficient after approximately 30 min. This phenomenon could be linked to the formation of Cr_2O_3 during the friction processes, which appears to possess some lubricating properties that help reduce wear. The average coefficients of friction measured for 304 stainless steel, TiBN, CrAlN, and CrAlN/TiBN are found to be 0.455, 0.642, 0.491, and 0.489, respectively.

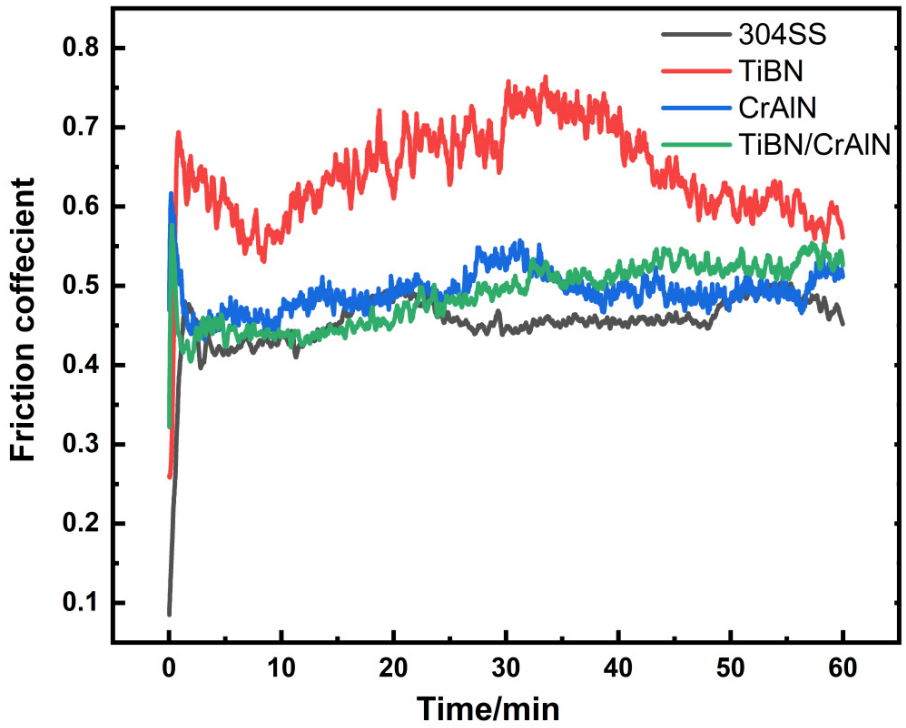

Figure 3. Variation of the friction coefficients of TiBN, CrAlN, and CrAlN/TiBN coatings with respect to testing time.

3.3. Corrosion Resistance of Coatings in Artificial Seawater

The corrosion medium utilized in this study is artificial seawater. The potentiodynamic polarization (Tafel) curves for the 304 stainless steel substrate and three types of coatings are illustrated in Figure 4. Data analysis of these polarization curves yields values for open circuit potential (E_{corr}) and corrosion current density (I_{corr}), as presented in Table 3. The corresponding self-corrosion potentials E_{corr} and corrosion currents I_{corr} for each coating are detailed therein. Based on the process parameters employed during the arc ion plating technology to fabricate these coatings, it can be inferred that all coatings act as dielectric layers with micro-pores on their surfaces. Consequently, their protective effect on the substrate primarily manifests through mechanical isolation. The self-corrosion potential reflects the equilibrium state between anodic and cathodic reactions at a metal surface under no external voltage, indicating its propensity to undergo corrosive reactions [30–34]. A higher value signifies a reduced likelihood of such reactions occurring. As depicted in Figure 4 and summarized in Table 3, there is a significant positive shift in self-corrosion potentials for all three coatings when compared to that of the 304 stainless steel substrate. Specifically, the self-corrosion potentials for 304 stainless steel, TiBN coating, CrAlN coating,

and CrAlN/TiBN coating are −0.3544 V, −0.1757 V, −0.075 V, and −0.0021 V, respectively. Among these samples tested, the CrAlN/TiBN coating exhibits the highest self-corrosion potential, which suggests that it possesses relatively low electrochemical activity within an artificial seawater corrosive environment.

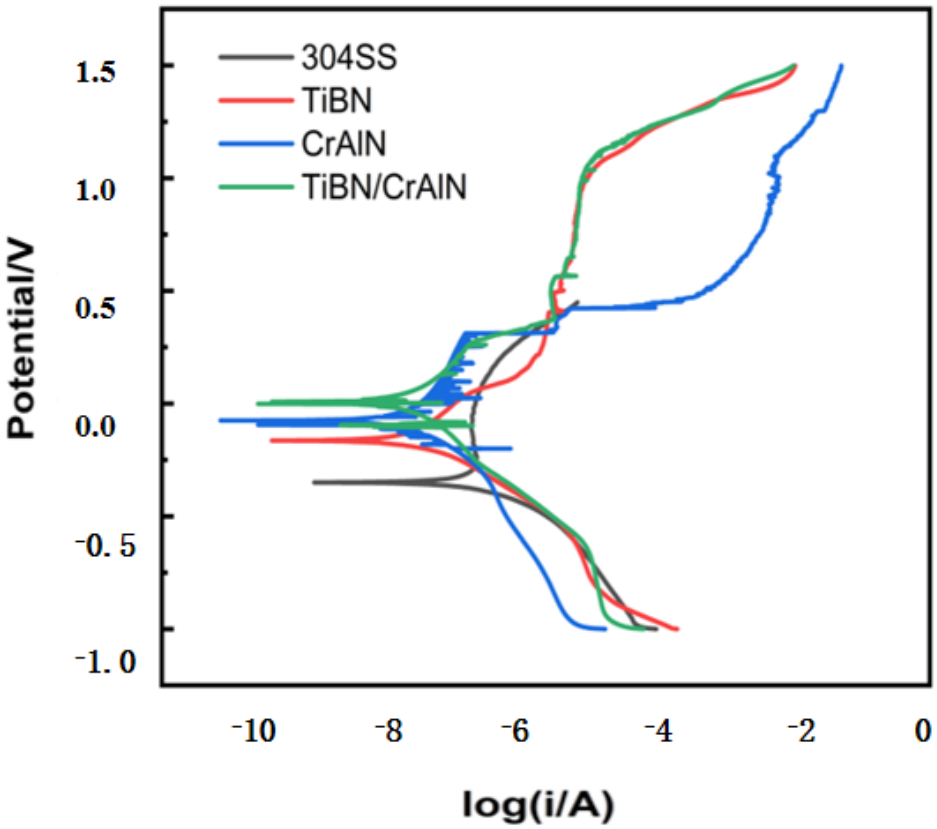

Figure 4. Tafel curves for coatings of 304 stainless steel, TiBN, CrAlN, and CrAlN/TiBN.

Table 3. Polarization curve corrosion parameters of 304 stainless steel, TiBN, CrAlN, and CrAlN/TiBN coatings.

Sample	$J_{corr}/(10^{-7}A \cdot cm^{-2})$	E_{corr}/V
304SS	3.816	−0.3544
TiBN	0.4732	−0.1727
CrAlN	0.2456	−0.075
TiBN/CrAlN	1.144	0.0021

The electrochemical impedance spectroscopy (EIS) tests were conducted in an artificial seawater solution, serving as the corrosive medium. In Figure 5, we present the Nyquist plot, while Figure 6 showcases the Bode plot. The Nyquist plots for TiBN, CrAlN, and CrAlN/TiBN coatings reveal two distinct time constants associated with incomplete capacitive resistance; one corresponds to a larger capacitive loop, whereas the other is represented by a smaller diameter capacitive arc [35]. From our EIS results, it becomes clear that TiBN, CrAlN, and CrAlN/TiBN exhibit two different interfacial reactions occurring at both the coating–solution interface and the substrate–coating interface, as illustrated in Figure 7b. We utilized ZsimpWin fitting software (https://www.ameteksi.com/products/software/zsimpwin, accessed on 4 November 2024) to analyze the EIS data while ensuring an error margin within 5%. The equivalent circuit model is depicted in Figure 7. In this model, CPE1 and CPE2 represent non-ideal capacitances. Rs denotes the solution resistance between the working electrode and the reference electrode, Rpo signifies pore resistance related to charge transfer during corrosion

reactions, and Rct represents charge transfer resistance pertinent to corrosion processes. Within the frequency range of 1 Hz to several kHz, Bode plots consistently demonstrate a linear increase until reaching the maximum phase angle before transitioning into a plateau stage. This behavior indicates that CPEs dominate in this region. Notably, among all tested coatings, CrAlN/TiBN exhibits the highest phase angle value, followed closely by the CrAlN coating. This observation suggests that CrAlN/TiBN possesses superior corrosion resistance compared to other evaluated coatings.

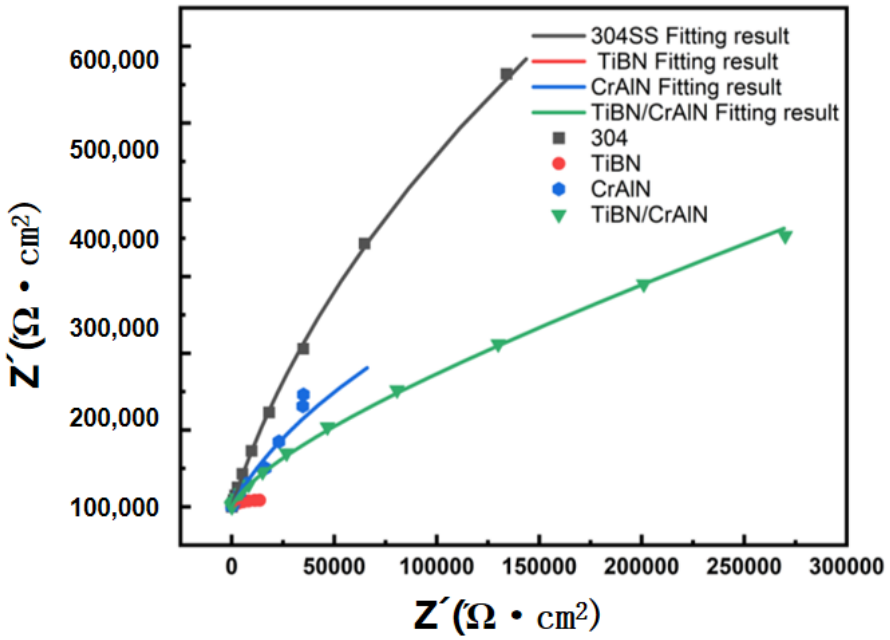

Figure 5. Nyquist curves of 304 stainless steel, TiBN, CrAlN, and CrAlN/TiBN coatings.

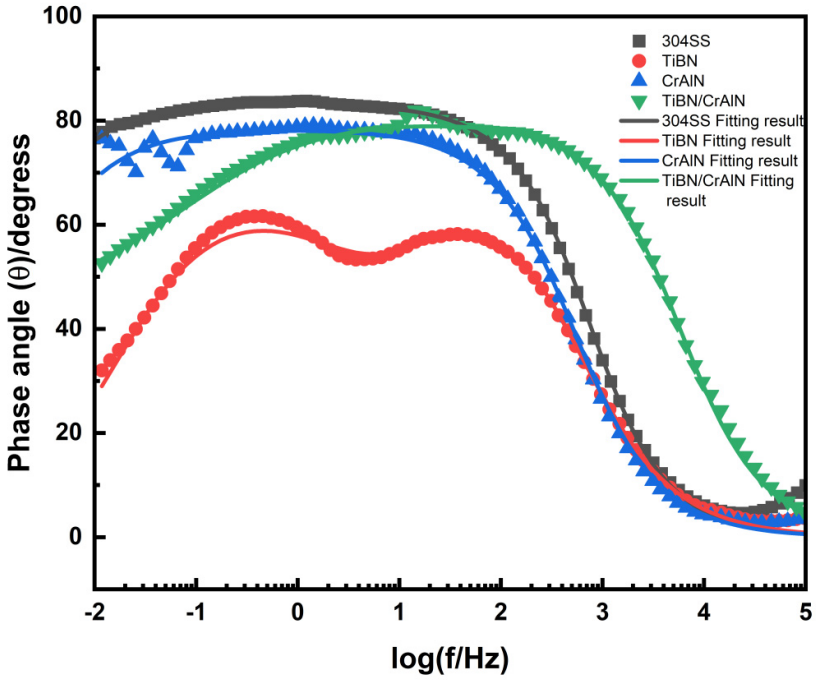

Figure 6. Bode angle curves for coatings of 304 stainless steel, TiBN, CrAlN, and CrAlN/TiBN.

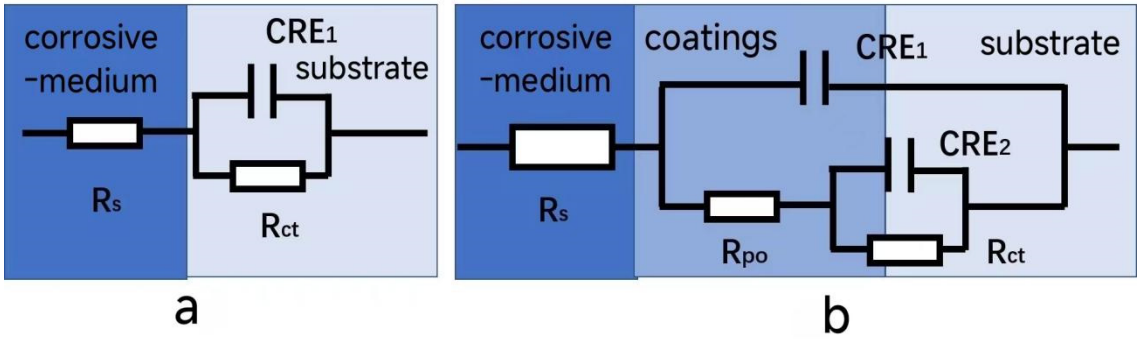

Figure 7. Results of AC impedance testing: (**a**) equivalent circuit used to fit the AC impedance spectrum of the 304 stainless steel coating; (**b**) equivalent circuit employed for fitting the AC impedance spectra of TiBN, CrAlN, and CrAlN/TiBN coatings.

4. Conclusions

In the present study, we employed arc ion plating technology to deposit TiBN, CrAlN, and nano-multilayer of CrAlN/TiBN. The surface and cross-sectional morphology, tribological performance, and electrochemical corrosion resistance of the three coatings were investigated. The results indicate that the preferred orientation of the TiBN coating is TiB_2 (101), while for the CrAlN coating, it is Cr(Al)N (200). In contrast, the preferred orientation for the CrAlN/TiBN multilayer coating is also TiB_2 (101). The multilayer structure refines grain size and disrupts columnar grain growth, resulting in a denser microstructure at the cross-section of these coatings. Tribological testing demonstrated that the friction coefficient follows this order: CrAlN/TiBN (0.489) > CrAlN(0.491) > TiBN (0.642), with CrAlN/TiBN exhibiting the lowest friction coefficient. Electrochemical tests conducted in artificial seawater showed that among these coatings, CrAlN/TiBN had the highest self-corrosion potential, followed by CrAlN. From the Bode plots analysis, it can be concluded thatCrAlN/TiBN displayed a maximum phase angle compared to other coatings. Due to its superior corrosion resistance properties, CrAlN/TiBN holds significant application value for protective measures on underwater breathing gas cylinders. The subsequent research will focus on the fatigue characteristics of coatings and the interactions between corrosion and friction. Additionally, a more diverse range of substrates, such as AISI 316, aluminum alloys, and carbon steel, will be used.

Author Contributions: Investigation, F.Y., Y.Y., Y.L., Y.X. and C.Z.; Writing—original draft, F.Y. and C.Z.; Project administration, F.Y. All authors have read and agreed to the published version of the manuscript.

Funding: This work was supported by the Innovation Team Project of Guangdong Universities (2020KCXTD032), Lingnan Normal University (LT2203), and the Science and Technology Projects of Zhanjiang (2022A0100, 2022B01044, 2024B01117).

Institutional Review Board Statement: Not applicable.

Informed Consent Statement: Not applicable.

Data Availability Statement: Data are contained within the article.

Conflicts of Interest: The authors declare no conflict of interest.

References

1. Chamberlin, R.E.; Guzas, E.L.; Ambrico, J.M. Energy balance during underwater implosion of ductile metallic cylinders. *J. Acoust. Soc. Am.* **2014**, *136*, 2489–2496. [CrossRef] [PubMed]
2. Dynamic implosion of underwater cylindrical shells: Experiments and computations. *Int. J. Solids Struct.* **2013**, *50*, 2943–2961. [CrossRef]
3. Study of implosion of carbon/epoxy composite hollow cylinders using 3-D digital image correlation. *Compos. Struct.* **2015**, *119*, 272–286. [CrossRef]

4. Gupta, S.; Matos, H.; LeBlanc, J.M.; Shukla, A. Shock initiated instabilities in underwater cylindrical structures. *J. Mech. Phys. Solids* **2016**, *95*, 188–212. [CrossRef]
5. Li, L.; Liu, L.L.; Li, X.; Guo, P.; Ke, P.; Wang, A. Enhanced tribocorrosion performance of Cr/GLC multilayered films for marine protective application. *ACS Appl. Mater. Interfaces* **2018**, *10*, 13187–13198. [CrossRef] [PubMed]
6. Wu, D.; Guan, Z.; Cheng, Q.; Guo, W.; Tang, M.; Liu, Y. Development of a friction test apparatus for simulating the ultra-high pressure environment of the deep ocean. *Wear* **2020**, *452*, 203294. [CrossRef]
7. Shan, L.; Wang, Y.; Zhang, Y.; Zhang, Q.; Xue, Q. Tribocorrosion behaviors of PVD CrN coated stainless steel in seawater. *Wear* **2016**, *362*, 97–104. [CrossRef]
8. Zhou, F.; Adachi, K.; Kato, K. Friction and wear behavior of BCN coatings sliding against ceramic and steel balls in various, environments. *Wear* **2006**, *261*, 301–310. [CrossRef]
9. Zuo, B.; Yu, L.; Xu, J. The new nanocapsule structure and cyclic tribological properties of $Mo_2N/Ag/Si_3N_4$ nanocomposite film. *Ceram. Int.* **2023**, *49*, 38982–38994. [CrossRef]
10. Zuo, B.; Yu, L.; Xu, J. Effect of Ag content on friction and wear properties of TiCN/Ag films in different service environments. *Vacuum* **2023**, *212*, 112029. [CrossRef]
11. Han, H.; Wu, T.; Zhao, L. Stable and durable TiBN-Cu/polyalphaolefin(PAO) composite lubrication system: Enhanced lubrication performance through PAO physicochemical adsorption. *Surf. Coat. Technol.* **2024**, *489*, 131093.
12. Neidhardt, J.; O'Sullivan, M.; Reiter, A.E.; Rechberger, W.; Grogger, W.; Mitterer, C. Structure property performance relations of high-rate reactive arc-evaporated Ti-B-N nanocomposite coatings. *Surf. Coat. Technol.* **2006**, *201*, 2553–2559. [CrossRef]
13. Bian, S.; Yu, L.; Xu, J.; Xu, J. Impact of Ag on the microstructure and tribological behaviors of adaptive ZrMoN-Ag composite lubricating films. *J. Mater. Res. Technol.* **2022**, *19*, 2346–2355. [CrossRef]
14. Wang, L.; Zhang, G.; Wood, R.J.; Wang, S.C.; Xue, Q. Fabrication of CrAlN Nanocomposite Films with High Hardness and Excellent Anti-wear Performance for Gear Application. *Surf. Coat. Technol.* **2010**, *204*, 3517–3524. [CrossRef]
15. Ning, L.; Veldhuis, S.C.; Yamamoto, K. Investigation of wear behavior and chip formation for cutting tools with nano-multilayered TiAlCrN/NbN PVD coating. *Int. J. Mach. Tools Manuf.* **2008**, *48*, 656–665. [CrossRef]
16. Adesina, A.Y.; Gasem, Z.M.; Madhan Kumar, A. Corrosion resistance behavior of single-layer cathodic arc PVD nitride-base coatings in 1M HCl and 3.5 pct NaCl solutions. *Metall. Mater. Trans. B* **2017**, *48*, 1321–1332. [CrossRef]
17. Li, S.; Liu, Y.; Guo, P.; Sun, L.; Ke, P.; Wang, A. Research Progress on Nitrogen/Carbon-Based Wear-Resistant Coatings via Physical Vapor Deposition in Marine Environments. *Surf. Technol.* **2021**, *50*, 44–56.
18. Yu, L.; Luo, H.; Bian, J.; Ju, H.; Xu, J. Research on microstructure, mechanical and tribological properties of Cr-Ti-BN films. *Coatings* **2017**, *7*, 137. [CrossRef]
19. Tian, C.; Xiang, Y.; Zou, C.; Yu, Y.; Abudouwufu, T.; Yang, B.; Fu, D. Mechanical and Tribological Properties of CrWN/MoN Nano-Multilayer Coatings Deposited by Cathodic Arc Ion Plating. *Coatings* **2024**, *14*, 367. [CrossRef]
20. Li, M.; Yu, Y.; Zou, C.; Tian, C.; Xiang, Y. Study on Friction and Corrosion Performance of CrTiBN Coating in Artificial Seawater Environment. *Coatings* **2023**, *13*, 1837. [CrossRef]
21. Kainz, C.; Schalk, N.; Tkadletz, M.; Mitterer, C.; Czettl, C. Microstructure and mechanical properties of CVD TiN/TiBN multilayer coatings. *Surf. Coat. Technol.* **2019**, *370*, 311–319. [CrossRef]
22. Anusha, T.V.V.; Chukwuike, V.I.; Shtansky, D.V.; Subramanian, B. Biocompatibility study of nanocomposite titanium boron nitride (TiBN) thin films for orthopedic implant applications. *Surf. Coat. Technol.* **2021**, *410*, 126968.
23. Yu, Y.; Li, M.; Zou, C.; Tian, C.; Xiang, Y. Effect of CrYN/TiBN coating on friction performance and corrosion resistance of 316 stainless steel in artificial seawater. *Mater. Res. Express* **2023**, *10*, 036506. [CrossRef]
24. Landolt, D.; Mischler, S.; Stemp, M. Electroc-hemical Methods in Tribocorrosion: A Critical Appr-aisal. *Electrochim. Acta* **2001**, *46*, 3913–3929. [CrossRef]
25. Li, W.; Sun, X.; Wang, Y.; Li, J.; Wang, C.; Sui, Y.; Lan, J. Study on the Corrosion and Wear Performance of Multi-Interface CrN/CrAlN Coatings in Seawater Environment. *Surf. Technol.* **2022**, *51*, 69–78.
26. Aihua, L.; Jianxin, D.; Haibing, C.; Yangyang, C.; Jun, Z. Friction and wear properties of TiN, TiAlN, AlTiN and CrAlN PVD nitride coatings. *Int. J. Refract. Met. Hard Mater.* **2012**, *31*, 82–88. [CrossRef]
27. Zhou, S.Y.; Yan, S.J.; Han, B.; Yang, B.; Lin, B.Z.; Zhang, Z.D.; Ai, Z.W.; Pelenovich, V.O.; Fu, D.J. Influence of modulation period and modulation ratio on structure and mechanical properties of TiBN/CrN coatings deposited by multi-arc ion plating. *Appl. Surf. Sci.* **2015**, *351*, 1116–1121. [CrossRef]
28. Chen, M.; Wu, D.; Chen, W.; Zhang, S. Structural optimisation and electrochemical behaviour of AlCrN coatings. *Thin Solid Film.* **2016**, *612*, 400–406. [CrossRef]
29. Wang, L.; Sun, R.; Shan, L.; Wang, Y. Study on the Corrosion and Wear Behavior of CrAlN Coatings in Seawater Environment. *Tribol. Lett.* **2017**, *37*, 639–646.
30. Kok, Y.N.; Akid, R.; Hovsepian, P.E. Tribocorrosion Testing of Stainless Steel (SS) and PVD Coated SS Using a Modified Scanning Reference Electrode Technique. *Wear* **2005**, *259*, 1472–1481. [CrossRef]
31. Wang, J.Z.; Yan, F.Y.; Xue, Q.J. Tribological behavior of various polymer materials in seawater. *Sci. Bull.* **2009**, *54*, 3558–3564. [CrossRef]
32. Yan, X.P.; Bai, X.Q.; Yuan, C.Q. A discussion on the connotation, research scope and progress of marine tribology. *J. Mech. Eng.* **2013**, *49*, 95–103. [CrossRef]

33. Song, X.X.; Ouyang, J.J.; Zhao, J.Y.; Hu, D.K.; Chen, Y.J. Comparative study on the corrosion resistance of Cr/CrN and Cr/CrN/CrAlN coatings prepared by magnetron sputtering. *Surf. Technol.* **2020**, *49*, 272–280.
34. Liu, E.Y.; Zeng, Z.X.; Zhao, W.J. Research progress on integrated technology for corrosion wear resistance of metallic materials in seawater environments. *Surf. Technol.* **2017**, *46*, 149–157.
35. Xiang, Y.; Wang, Z.; Liu, G.; Liang, F.; Zou, C.; Yu, Y.; Tian, C. Preparation and wear-corrosion performance study of single-layer/multi-layer TiN-based coatings on the surface of 304 stainless steel. *Surf. Technol.* **2022**, *51*, 121–128.